Nanoscale

Accepted Manuscript

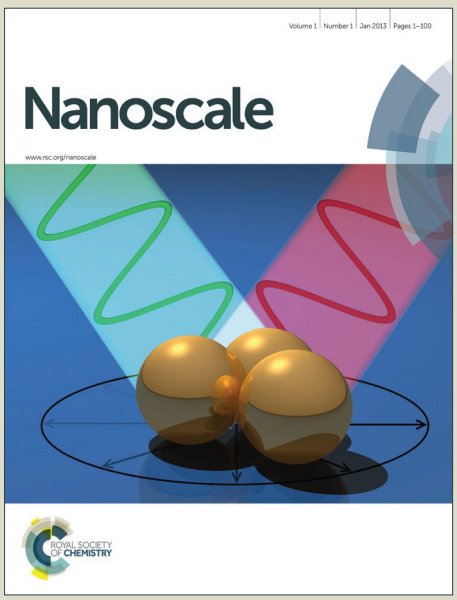

ROYAL SOCIETY OF CHEMISTRY

www.rsc.org/nanoscale

Journal Name

ARTICLE

A highly sensitive, low-cost, wearable pressure sensor based on conductive hydrogel spheres †

Received 00th January 20xx,
Accepted 00th January 20xx

DOI: 10.1039/x0xx00000x

www.rsc.org/

Yanlong Tai, Matthieu Mulle, Isaac Aguilar Ventura, Gilles Lubineau*

Wearable pressure sensing solutions have a promising future for practical applications in health monitoring and human/machine interfaces. Here, a highly sensitive, low-cost, wearable pressure sensor based on conductive single-walled carbon nanotube (SWCNT)/alginate hydrogel spheres is reported. Conductive and piezoresistive spheres are embedded between conductive electrodes (indium tin oxide-coated polyethelene terephthalate films) subjected to environmental pressure. The detection mechanism is based on the piezoresistivity of the SWCNT/alginate conductive spheres and on the sphere-electrode contact. Step-by-step, we optimized the design parameters to maximize the sensitivity of the sensor. The optimized hydrogel sensor exhibited a satisfactory sensitivity (0.176 $\Delta R/R_0$ /kPa^{-1}) and a low detectable limit (10 Pa). Moreover, a brief response time (a few milliseconds) and successful repeatability were also demonstrated. Finally, the efficiency of this strategy was verified through a series of practical tests such as monitoring human wrist pulse, detecting throat muscle motion or identifying the location and the distribution of an external pressure using an array sensor (4×4)

1. Introduction

In recent years, wearable electronics that can detect changes in human blood pressure are drawing considerable attention. These new kinds of flexible, skin-like sensors transduce pressure variations into electronic signals [1-5]. Such sensors need to be capable of operating in the range of frequency and pressure amplitude defined by natural physiological fluctuations (e.g., heart rate and blood pressure). Although a simple relationship between blood pressure and specific health conditions has not yet been established, it is widely accepted that they are closely related. Thus, it is important to accurately investigate how to measure subtle changes during cycles of pulse pressure variation. Highly sensitive, portable pulse pressure sensors need to be developed for the efficient diagnosis of disease and general health monitoring. In addition to health monitoring, sensitive pressure sensors can also be used in many other applications including voice recognition and human/machine interfaces by analyzing signals from human throat muscle movement [6-9].

To date, the sensing mechanisms of pressure sensors have been based primarily on changes in capacitance [10-12], piezoelectricity [13-15], piezoresistivity [3, 6, 16-19] and triboelectricity [20-23]. Although some conventional silicon-based sensors exhibit a high resolution (0.5 Pa), they show poor wearability, have high manufacturing costs and are not environmental friendly [6, 24-28]. Currently, several technologies for flexible pressure sensors have been reported: polydimethylsiloxane (PDMS) and carbon nanotube (CNT) nanosheet-based sensors [6], ultrathin Au nanowire-based piezoresistive sensors [9], nanowire active array field-effect transistors [16] and microstructured rubber dielectric layer capacitors [29]. However, these techniques all encounter similar problems: fabrication of complicated microstructures and nanostructures, difficult upscaling, high costs and require the use of materials that maybe difficult to procure or produce. Thus, the design and manufacture of wearable, highly sensitive, reproducible and cost-effective pressure sensors for a variety of applications continues to be a challenge. Here, we aim to develop simply designed, low-cost bio-based sensors that are easily manufactured by controlling both the geometry and the intrinsic properties of the materials.

Alginate is a common natural polysaccharide that is made of β-D-mannuronic acid (M) and α-L-guluronic acid (G). Because it is highly water soluble, biocompatible and nontoxic, it has been widely used in food, medicine, personal care products and wastewater treatment [30]. One of its key features is its capacity to react with multivalent cations to form a hydrogel via crosslinking mechanisms. It can easily be shaped into different geometries, and by adjusting the M/G content ratio [31] it can be tailored to cover a wide range of viscoelastic and mechanical properties. The properties of the hydrogel can be further customized by adding nanofillers such as CNTs or graphene [32]. Despite its attractive characteristics (e.g.,

King Abdullah University of Science and Technology (KAUST), Physical Sciences and Engineering Division, COHMAS Laboratory, Thuwal 23955-6900, Saudi Arabia.
**E-mail: gilles.lubineau@kaust.edu.sa*
†Electronic Supplementary Information (ESI) available: [details of any supplementary information available should be included here]. See DOI: 10.1039/x0xx00000x

tunability, biocompatibility and availability), alginate has never been used in the design of pressure sensors for healthcare applications.

Here, we report the development of a pressure sensor technology based on single-walled (SW) CNT/alginate hydrogel spheres. We explore different sensing mechanisms and perform a sensitivity optimization technique to develop the most progressive technology.

First, the conductivity of alginate-based hydrogel was improved by doping with SWCNTs, which is necessary for the device to operate at low voltages. We performed an in depth study of the change in hydrogel electrical resistance with various doping configurations. Our results allowed us to determine the concentration of SWCNTs closest to the percolation threshold to simultaneously promote high conductivity and a strong piezoresistive effect.

Second, we used this SWCNT-doped alginate hydrogel to synthesize hydrogel spheres, which were further sandwiched between indium tin oxide- (ITO) coated polyethylene terephthalate (PET) films such that a small preload could be applied to the sphere. The preload created a contact geometry that can easily be disturbed under external mechanical pressure. Both the changes in material properties and in contact geometry will contribute to the sensing response (Fig. 1a). The relative contributions of contact resistance (R_c) at the hydrogel sphere-electrode interface and of piezoresistance (R_s) of the hydrogel sphere were determined.

Third, we evaluated the performance of this sensor through the analysis of several design parameters. The mechanical-resistance response was characterized with different loading values, frequencies and cycles. We show that, depending on sensor parameters, the sensor has a high sensitivity, a fast mechanical-electronic response, successful repeatability and a low pressure-detecting limit.

Finally, the efficiency of this strategy was verified through a series of practical tests, illustrating some possible applications. In the first step, a single-sphere hydrogel sensor was tested for human wrist pulse monitoring and throat muscle motion detection. Next, a skin-like array sensor (4x4) was developed and tested to detect the location and distribution of an external pressure.

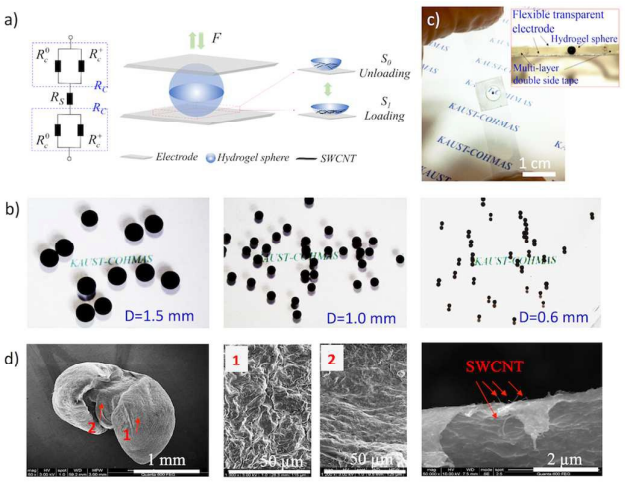

Fig.1 a) Schematic illustration of the sensing system based on conductive hydrogel spheres and its equivalent electrical circuitry (Rc: equivalent contact resistance, R_C^0: initial contact resistance without any loading, R_C^+ : resistance of the additional contact surface under pressure, Rs: hydrogel sphere resistance); b) conductive SWCNT/alginate hydrogel spheres with different diameters; c) typical configuration of a hydrogel sensor; d) SEM of different parts of a conductive SWCNT/alginate hydrogel sphere (1 and 2 are surface and internal morphology, respectively, of a hydrogel sphere cut with a scalpel).

2. Experimental

2.1 Materials

Sodium alginate powder was purchased from Qingdao Mingyue Company (China) with a viscosity of 150-200 cps. Carboxyl group (−COOH) functionalized SWCNTs were purchased from CheapTubes Inc. with an outer diameter of 1-2 nm, a length of 5-30 µm and over 95 wt. % purity or 2.56 wt. % of COOH groups. ITO-coated PET films were purchased from Sigma-Aldrich (sheet resistance = 60 ohm/sq, PET thickness = 125 µm, ITO thickness = 130 nm and transmittance > 79 % at 550 nm of wavelength). Calcium chloride was also purchased from Sigma-Aldrich. Deionized water was used in all experimental procedures.

2.2 Synthesis of SWCNT/alginate hydrogels

The SWCNT/alginate conductive solution was prepared according to the following four-step procedure. The desired amount of SWCNTs and sodium alginate (0.5 g) was added to deionized water (100 g). The solution was then homogenized by sonication at 20 kHz and 500 W for 30 min followed by magnetic stirring at high speed for 2 h on a hotplate (80 ℃). Next, additional sodium alginate (2.5 g) was added to the prepared mixture and the solution was blended for 6 h with the same conditions described above. And finally, the solution was used to prepare either SWCNT/alginate hydrogel films or SWCNT/alginate hydrogel spheres.

SWCNT/alginate hydrogel films were prepared according to the following procedure. Two glass slides were assembled face-to-face, spaced according to the thickness of double-sided tape. The slides formed a mold that was filled with the prepared alginate solution using a syringe. Next, the setup was immersed in the calcium chloride solution (5 wt. %) for 6 h. And finally the hydrogel film was removed from the laminated glass slides with tweezers (Fig. S1a).

SWCNT/alginate hydrogel spheres were prepared by the following procedure. Drops of the prepared SWCNT/alginate solution were injected into the calcium chloride solution (5 wt. %) with a Thermo Scientific Finnpipette (0.2 - 2 µl), as shown in Fig. 1b. When the droplet volumes were 0.2 µl, 0.6 µl and 1.9 µl, the final diameters of the hydrogel sphere were 0.6 ± 0.005 mm, 1.0 ± 0.005 mm and 1.5 ± 0.005 mm, respectively, after allowing gelation for 6 h in the calcium chloride solution.

SWCNT/alginate hydrogel cylinders were prepared as described below. Cylinders with 3 ± 0.2 mm diameters = were prepared by continuously injecting the SWCNT/alginate solution into the calcium chloride solution (5 wt. %) using a syringe (10 ml container, no needle). We cut cylinders of different lengths, depending on the test they will be used for (Fig. S1b, S1c and S1d).

2.3 Pressure-sensing device fabrication

Single hydrogel sensors were prepared by the following procedure. The prepared SWCNT/alginate hydrogel spheres were sandwiched between ITO-coated PET films. The sphere was positioned in the center of a circular hole made in a stack of multiple layers of double-sided tape (single-layer thickness = 100 µm and a hole diameter = 6 mm). Stack of 6 (0.593-mm thick), 10 (0.987-mm thick) or 15 layers (1.480-mm thick) of double-sided tape were used to produce hydrogel spheres with diameters of 0.6, 1.0 or 1.5 mm, respectively. The difference between the thickness of the stacked double-sided tape and the diameter of hydrogel sphere induces a small preload to ensure contact between the hydrogel sphere and the ITO-coated PET electrodes. Copper wires were bonded on the surface of the ITO-coated PET using silver paste, which was then cured on a hot plate at 100 °C for 1 h. Fig. 1c shows the typical configuration of a hydrogel sensor.

Skin-like array sensors were prepared using the following technique: For the lower skin, a 4×4 ITO electrode array (electrodes are circular with a diameter = 6 mm and distances between each = 8 mm) was patterned on PET film by shadow mask lithography. For the upper skin, a normal ITO-coated PET film of the same size was used. Then, a 10-layer stack of double-sided tape with 6-mm diameter holes was bonded to the lower skin. The prepared hydrogel spheres (diameter = 1 mm and number = 16) were positioned in the center of each hole, and the upper skin was set symmetrically to cover all spheres. And finally, each electrode (16 circular electrodes in the lower skin and one electrode in the upper skin) was connected to copper wires using silver paste. More details are presented in Fig. 2.

Fig. 2 The skin-like pressure sensor. a) The fabrication process, b) a photograph of the sensor and c) the schematic equivalent electric circuit.

2.4 Characterization and measurements

The morphology of synthesized SWCNT/alginate hydrogels was examined by scanning electron microscopy (SEM, Quanta 600, FEI Company) (Fig. 1d). We investigated the chemical structure using a Fourier transform infrared Nicolet iS10 spectrometer (FTIR, Thermo Fisher Scientific, Inc.) and sheet resistance using the 4-point probe system (Pro4-440N, Lucas Labs). For the real-time mechanical-resistance response, we used a PC-controlled universal test machine (UTM, Instron 5944 with a 5 N load cell, ± 0.5 % of reading down to 1/250 to the load cell capacity) and a PC-recordable multimeter (Agilent 34401A).

To ensure that the pressure was evenly distributed over the entire functional area, special care was taken to design the mechanical interface between the UTM tip and the sensor surface. A very soft polyurethane sponge (2-mm thick) was inserted between the UTM tip and the sensor to provide a transition layer. Here, we describe a method of preloading 0.02 N to ensure satisfactory initial contact (Fig. 3a and 3b). Thus, the pressure (P) is the ratio of the UTM loading (F) and the contact area (square with the dashed red outline) that includes the edges of the sensor and the sensing area (the contact area here was 1 cm^2). The mechanical-resistance response was recorded as we described above. We tested the efficiency of the array sensor by applying pressure with a finger at different locations.

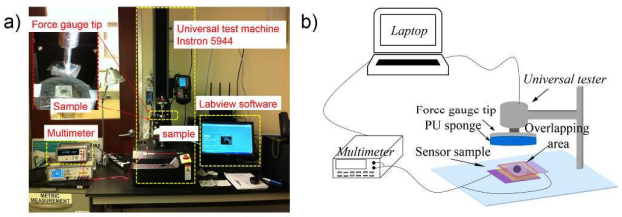

Fig. 3 The measurement setup to investigate the mechanical-resistance response.

3. Results and discussion

3.1 Theoretical analysis

Fig. 1a illustrates the structure of the designed sensor.

The hydrogel sphere was considered to be a resistive element (R_s). The hydrogel sphere is conductive because of the free ions (including calcium ion (Ca^{2+}), sodium ion (Na^+), and chloride ion (Cl^-)). The current (I) - voltage (V) property of the as-prepared sensor was investigated to determine the equivalent macroscopic mechanism. As shown in Fig. S2, the I/V relationship for both the pure alginate sensor and SWCNT/alginate sensor is almost linear, indicating that the macroscopic behavior can be approximated as ohmic. The almost linear curves also suggest the existence of a non-ohmic part [10, 33, 34], which can yet be neglected from a macroscopic point of view.

The contact resistance (R_c) between the hydrogel sphere and the electrode was also considered. We assumed that the contact resistance was related to the sphere/electrode contact surface, which can be predicted from Hertz's contact theory (Supporting Information, Section S1). The contact resistance results from the initial contact resistance (R_C^0) on the resistance of the additional contact surface created under pressure (R_C^+).

The change in the total resistance is thus based on the change in the contact resistance of the hydrogel sphere-electrode interface and the piezoresistive effect of the hydrogel sphere. We demonstrate in the supporting information (Fig. S3) that the change in the contact resistance is the main mechanism.

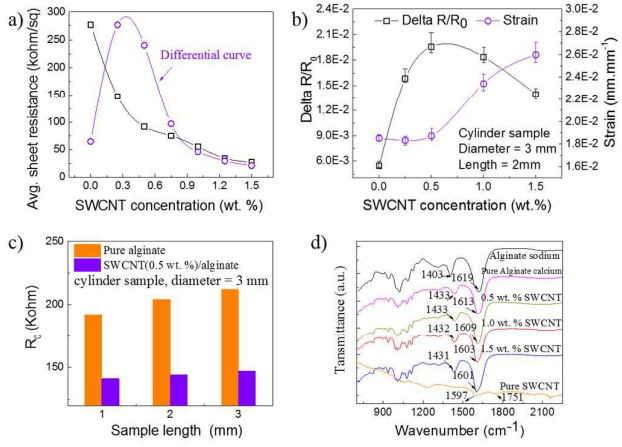

Fig. 4 Characterization of the sensing SWCNT/alginate hydrogel. a) Sheet resistance of SWCNT/alginate hydrogel film with different concentrations of SWCNTs; b) mechanical-resistance/strain response of SWCNT/alginate hydrogel cylinders at different concentrations of SWCNTs (preload = 0.01 N, cycle load = 0.05 N); c) total resistance as a function of alginate cylinder length (gold-coated wafer as electrodes); d) FTIR spectra of SWCNTs, alginate sodium and SWCNT/alginate hydrogels at different concentrations of SWCNTs.

When an external load is applied against the lower or upper electrode, the conductive film deflects causing the hydrogel sphere to deform accordingly; this changes the contact area between the hydrogel sphere and the electrode. Initially, this contact area is almost pointwise, making it very sensitive to any pressure variation. This directly affects R_c, whereas R_s is affected by the resistance sensitivity of the hydrogel sphere.

3.2 Optimizing the sensing material

The material for the spheres was first optimized to increase both its volume electrical conductivity and its piezoresistivity. Films of alginate-based hydrogel were made with different concentrations of SWCNTs ranging from 0 to 1.5 wt. %. Sheet resistance was then systematically measured by a 4-probe technique to investigate the change in electrical conductivity. Fig. 4a shows a distinct improvement in electrical conductivity as the sheet resistance decreased from 275 kohm/sq for the pure alginate gel to 25 kohm/sq for the 1.5 wt. % configuration. This improvement in electrical conductivity is important for operating the device at relatively low voltages. A classical percolation behavior was observed between 0.2 to 0.6 wt. %, as evidenced by the differential curve of sheet resistance (Fig. 4a).

Next, to maximize the piezoresistive response, we needed to select a concentration of SWCNTs close to the percolation threshold. In this domain, the percolated network is highly strain sensitive due to the easy perturbation of the tunneling effect between nanoparticles. To further confirm this hypothesis, the relative change in resistance ($\Delta R/R_0$, where R_0 is the original resistance) of cylinder samples (diameter = 3 mm and length = 2 mm) was investigated when they were compression-loaded under similar forces (0.05 N). As shown in Fig. 4b, a maximum relative change in resistance of 0.021 was obtained when the concentration of SWCNTs in alginate was 0.5 wt. %. This variation was approximately 4-fold that observed for pure alginate (0.0054). Therefore, at 0.5 wt. % of SWCNTs, we obtained the most effective piezoresistive effect.

It is also important to determine which part of the sensor, R_s or R_c, contributes more to the total resistance and subsequently to the sensing mechanism. For this, we measured the total resistance of hydrogel cylinders of various lengths. Assuming that the contact resistance is constant, despite cylinder length, the total resistance of the setup (length, L; diameter, D) can be estimated though equation (1):

$$R_t = 2R_c + R_{bulk} = 2R_c + \rho\frac{4L}{\Pi D^2} \qquad (1)$$

Here, R_c is the contact resistance and ρ is the volume resistivity of the bulk material. From Fig. 4c, we can approximate R_c and ρ for pure alginate (R_c ≈ 185 kohm, ρ ≈ 104 ohm·m) and for SWCNT (0.5 wt. %)/alginate (R_c ≈ 131 kohm, ρ ≈ 22 ohm·m). In this way, the global resistance will always be guided by the contact resistance, which will become the main sensing mechanism in the next section.

We found it interesting that SWCNTs modified the mechanical properties of the alginate hydrogel. We measured the strain change of SWCNT/alginate hydrogels under compression throughout the experiments described above, and the results are summarized in Fig. 4b. We report here the maximum strain achieved at a maximum compressive load (0.05 N). Considering that we are operating well below the plasticity limit and that viscous relaxation remains small at the considered time scale, strain at the maximum load can be considered primarily as a result of elastic deformation. Despite that a small stiffness increase was observed for very low SWCNT loading (0.25 wt. %), the addition of SWCNTs appears to rapidly become detrimental to the stiffness, as the elastic modulus decreases up to 30 % when adding 1.5 wt. % SWCNTs (maximum strain increases from 8.0 ×10^{-3} to 2.6 × 10^{-2}). At low loading pressures, the positive effect can be ascribed to restrictions in the mobility of the polymer chains. At higher loading pressures, we suspect that a high density of SWCNTs prevents crosslinking of the alginate solution by the ionic species, resulting in an overall reduction of the macroscopic mechanical properties; [35, 36] results from the FTIR test (Fig. 4d) offer some support for this assumption. The FTIR spectra appear not to be significantly modified by the introduction of various concentrations of SWCNTs. This denotes the absence of strong chemical bonding between the alginate chains and the SWCNTs. Instead, weak physical bonding (Van der Waals forces or hydrogen bonding) takes place, which does not translate into any reinforcement of the SWCNTs. Thus, the addition of SWCNTs only causes disruption to the ionic crosslinking.

Finally, the SWCNT- (0.5 wt. %) alginate configuration was selected to prepare hydrogel spheres for subsequent tests. Spheres with different diameters (0.6, 1.0 and 1.5 mm) were prepared as shown in Fig. 1b. SEM images of one sphere are presented Fig. 1c [37, 38]. The images show that the surface and internal morphologies are similar and that the SWCNTs are uniformly dispersed in the alginate matrix, which is a benefit for creating a quality conductive network.

3.3 Design and characterization of sensors

Design of the sensors is influenced by the physical properties of the membrane (e.g., thickness, Young's modulus or Poisson's ratio), the sensing area and the diameter of the hydrogel sphere. And, consequently the sensitivity of the sensors is largely dictated by its geometric design [39, 40]. Because the bulk of the variation is nondimensional, we decided to maintain some geometrical parameters constant to investigate only the effect of diameter on the hydrogel sphere.

The diameter of the sensing area was maintained at 6 mm and the thickness of the electrode membrane at 125 µm. Fig. 5a presents the results of the mechanical-resistance response of the hydrogel sensor with different diameters of hydrogel spheres (D = 0.6 mm, D = 1 mm and D = 1.5 mm). The resistance variations ($\triangle R_T/R_T^0$ = (R_T^0-R_T)/ R_T^0, where R_T^0 and R_T are the total resistances of the device without and with applied pressure, respectively) are plotted as a function of applied pressure (p). The pressure sensitivity, S, is the slope of the curves (S = δ ($\triangle R_T/R_T^0$)/ δ p). Because the curves are nonlinear, the sensitivity was calculated on two different segments and the results are listed in Table 1. We observed two main features: (1) the sensitivity of the sensor decreased as the pressure increased and (2) the sensitivity of the sensor decreased as the diameter of the sensing sphere increased.

These observations are consistent with piezoresistivity that is mainly guided by a change in the surface of the electrode-sphere contact area. The piezoresistive response of the constitutive material of the alginate sphere is very small, as demonstrated in Fig. S3. Following Hertz's theory, Equation (2) describes the change in resistance as a function of the applied pressure:

$$\frac{\Delta R}{R_T^0} = \frac{R_T^0 - R_T}{R_T^0} = \zeta p^{2/3} \quad (2)$$

where ζ is a reduced parameter that is explained in Supporting Information Section S1 with the full proof for Eq. 2. We can see from Equation (2) that the contact area is a power function of the applied pressure with a 2/3 exponent (Fig. S6). This is consistent with the change in sensitivity with pressure that we observed in Fig. 5a.

It is important to note that, as shown in Fig. 5a, the effective working range of the hydrogel sensor is from 0 Pa to 1000 Pa ~ 1400 Pa.

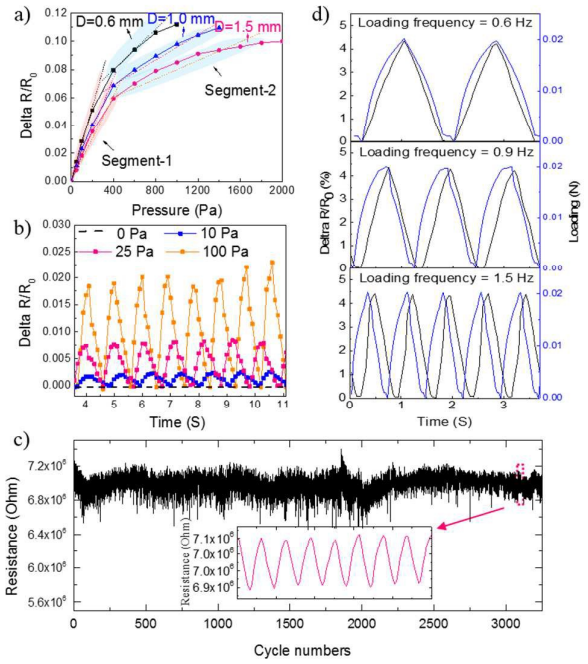

Fig. 5 Characterization of the mechanical-resistance response of the hydrogel sensor. a) Sensitivity of the sensor with different diameters of hydrogel spheres, b) short cyclic tests with different pressures and c) long cyclic tests under a dynamic force of 0.02 N. Response time at various cyclic loading frequencies are presented. Diameter of the hydrogel sphere is 1 mm, the displacement rate was 0.9 Hz, and all tests were preloaded at 0.02 N.

Table. 1 Sensitivity of the hydrogel sensor with different hydrogel spheres.

Diameter	Sensitivity (kPa^{-1})	
(mm)	Segment-1	Segment-2
0.6	0.398	0.071
1.0	0.176	0.041
1.5	0.149	0.015

We analyzed key properties of the pressure sensor that relate to monitoring continuous human pulse signals; for example, the lowest detectable pressure, the speed of the response and the service durability of the mechanism. These results are presented in Fig. 5b, 5c and 5d. To determine the lowest detectable limit, decreasing loadings were applied to the device until no resistance reading could be obtained; we found this value at 10 Pa (Fig. 5b). Meanwhile, at 25 Pa, a sharp signal with low noise and satisfying repeatability was observed.

To test the long-term stability of the sensor, we investigated its response when subjected to a rapidly varying cyclic loading (maximum loading: 0.02 N, loading frequency: 0.9 Hz). Results are presented in Fig. 5c. We found that a clear signal was maintained after 3000 cycles and the resistance amplitude exhibited negligible changes, proving adequate mechanical durability with no noticeable drift. In addition, for information, the initial resistance was measured on multiple devices based on a 1mm in diameter hydrogel sphere, showing a range of 6.9 × 10^6 - 7.4 × 10^6 ohm.

We applied a cyclic loading profile to the sensor at different frequencies to evaluate the dynamic response time to external loading, the cycle follows a waveform from 0 to 0.02 N. By comparing the output resistance signals to the applied force profile, we observed a gradual shift between loading and resistance curves with increasing frequency (Fig. 5d). When the displacement frequency was 1.5 Hz, the shift was less than 0.1 s. This phenomenon was expected and does not affect the overall sensing efficiency of the pressure device. Furthermore, this confirms that SWCNT/alginate hydrogels have a viscoelastic behavior.

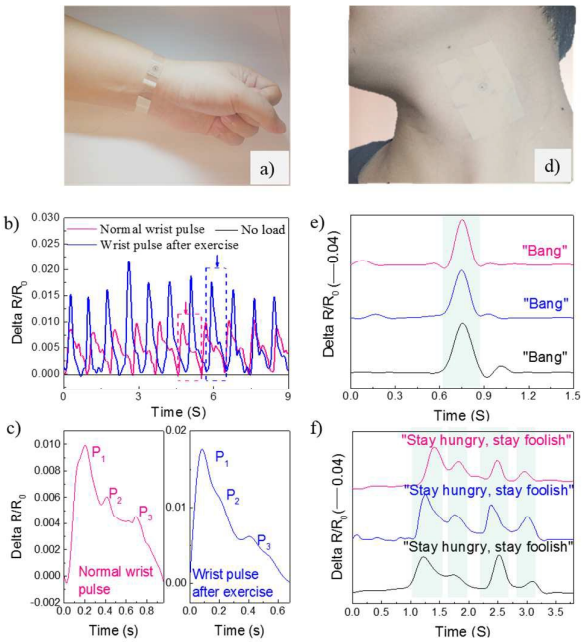

Fig. 6 Real-time monitoring of wrist pulses and neck muscle motion during speech. a) A digital image showing a wearable sensor directly attached to the artery of the tester's wrist. b) And c) resistance-response measurements of a human heartbeat at rest (61 beats/min) and following exercise (74 beats/min). d) A digital image showing the wearable sensor directly attached to the tester's neck. e) And f) resistance-response measurements for different words and phrases.

3.4 Detection of wrist pulses

The prepared sensor was tested for cardiovascular pressure assessment (Fig. 6a) by continuously tracking the pressure waveforms. Fig. 6b shows that the wrist pulses could be read

accurately at rest (61 beats/min) and after physical exercise (74 beats/min). At rest, a typical radial artery pulse waveform was obtained with two clearly distinguishable peaks (P_1 and P_3) and a late augmentation shoulder (P_2) (Fig. 6c). The shape of this curve is caused by the blood pressure generated by contractions of the left ventricle (P_1 and P_3) and a reflective wave from the lower body (P_2) [9, 10]. This data provides us with the radial augmentation index (P_2/P_1), which is an important value for characterizing arterial stiffness [41]. After physical exercise, the shapes of the pulse waves exhibited a subtle change in (P_2) that is related to late systolic augmentation [9]. These results confirm that our hydrogel sphere-based pressure sensors can identify subtle differences in blood pulses at the wrist, demonstrating their potential as a wearable diagnostic device to monitor human health in real-time.

3.5 Detection of muscle movement

Next, we attached the sensor to an individual's neck to monitor the pressure variation with muscle movement that occurs during speech (Fig. 6d). From Fig. 6e and 6f, we observed that the hydrogel sensor detected resistance variations when the speaker said and repeated different words such as "Bang" and "Stay hungry, stay foolish." The $\Delta R/R_0$-t curves for the same words or phrases had very similar profiles including characteristic peaks and valleys. These are mainly caused by deformation of the epidermis and the muscles around the throat while speaking. Therefore, the as-prepared hydrogel sensor may provide a promising and effective method for voice recognition or may provide assistance to people with damaged vocal cords.

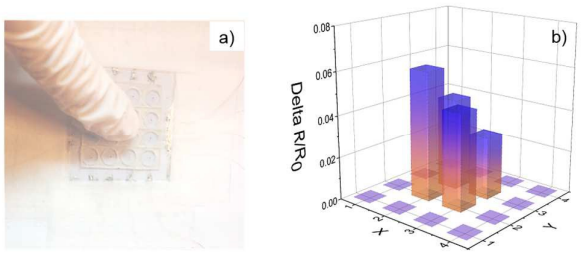

Fig. 7 a) A digital image of a finger applying pressure to the surface of the skin-like sensor. b) 3D graph of the in-plane distribution and amplitude of the resistance variation.

3.6 Skin-like array sensors

Fig. 7a shows a photo of the constructed skin-like array sensor. We measured the detection performance of the device by applying pressure with a finger on the surface of the sensor. The detected signal was recorded and plotted as a three dimensional (3D) graph of the in-plane distribution and amplitude of the resistance variation (Fig. 7b). This shows that pressure was distributed on several sensing units with different amplitudes, a typical feature of electronic skins [42, 43]. The skin-like sensor presented here has a centimeter-scale resolution, but it can also be reduced to a millimeter- or even a micrometer-scale resolution if an advanced photolithography technique is used.

Conclusions

We presented a simple method for the fabrication of highly sensitive, low-cost, wearable pressure sensors. This involves the preparation of a SWCNT/alginate hydrogel sphere, sandwiched between two conductive ITO-coated PET membranes. The unit had a sensing area diameter of 6 mm, a hydrogel sphere diameter of 1.0 mm and an electrode membrane thickness of 125 µm that resulted in a flexible device with sensitivity as high as 0.176 kPa^{-1} and a pressure detection limit as low as 10 Pa. A rapid mechanical-resistance response and successful repeatability were also demonstrated. By adding SWCNTs, performance was improved by approximately 10–15 % compared with pure alginate. The device showed very satisfying aptitudes for detecting human wrist pulse, and it was also used successfully for monitoring the real-time resistance response of throat muscle movement with different words or phrases, demonstrating its capacity for voice recognition. A skin-like array of these sensors was developed and exhibited impressive abilities to localize, quantify and reveal the distribution of external pressures. Furthermore, the techniques used to prepare these hydrogel spheres and fabricate the resulting pressure sensors could be translated into their production on an industrial-scale and at relatively low cost. Further investigations will be necessary to improve the thermal stability of sensors for maximized durability. Future directives include their practical application to health monitoring and human/machine interfaces.

Supporting Information

Acknowledgements

This research was supported by KAUST baseline funding. Authors are grateful to King Abdullah University of Science and Technology for its financial support.

References

1 E. Lumpkin, and M. Caterina, *Nature*, 2007, 445, 858.
2 Y. Joo, J. Byun, N. Seong, J. Ha, H. Kim, S. Kim, T. Kim, H. Im, D. Kim, and Y. Hong, *Nanoscale*, 2015, 7, 6208.
3 L. Pan, A. Chortos, G. Yu, Y. Wang, S. Isaacson, R. Allen, Y. Shi, R. Dauskardt, and Z. Bao, *Nat. Commun.*, 2014, 5, 3002.
4 D. Kim, N. Lu, R. Ma, Y. Kim, R. Kim, S. Wang, J. W. S. Won, H. Tao, A. Islam, K. Yu, T. Kim, R. Chowdhury, M. Ying, L. Xu, M. Li, H. Chung, H. Keum, M. McCormick, P. Liu, Y. Zhang, F. Omenetto, Y. Huang, T. Coleman, and J. Rogers, *Science*, 2011, 333, 838.
5 W. Wu, X. Wen, and Z. L. Wang, *Science*, 2013, 340, 952.
6 X. Wang, Y. Gu, Z. Xiong, Z. Cui, and T. Zhang, *Adv. Mater.*, 2014, 26, 1336.

7 J. Lee, S. Kim, J. Lee, D. Yang, B. Park, S. Ryua, and I. Park, *Nanoscale*, 2014, 6, 11932.
8 J. Park, Y. Lee, J. Hong, M. Ha, Y. Jung, H. Lim, S. Kim, and H. Ko, *ACS nano*, 2014, 8, 4689.
9 S. Gong, W. Schwalb, Y. Wang, Y. Chen, Y. Tang, J. Si, B. Shirinzadeh, and W, Cheng, *Nat. Commun*., 2014, 5, 3132.
10 B. Nie, R. Li, J. Brandt, and T. Pan, *Lab Chip*, 2014, 14, 1107.
11 J. Jeong, M. Kim, H. Cheng, W. Yeo, X. Huang, Y. Liu, Y. Zhang, Y. Huang, and J. Rogers, *Adv. Healthc. Mater*., 2014, 3, 621.
12 G. Schwartz, B. Tee, J. Mei, A. Appleton, D. Kim, H. Wang, and Z. Bao*, Nat. Commu*n., 2013, 4, 1859.
13 W. Choi, J. Lee, Y.K. Yoo, S. Kang, J. Kim, and J.H. Lee, *Appl. Phys. Lett*., 2014, 104, 123701.
14 C. Dagdeviren, Y. Su, P. Joe, R. Yona, Y. Liu, Y. Kim,Y. Huang, A. Damadoran, J. Xia, L. Martin, Y. Huang and J. Rogers, *Nat. Commun*., 2014, 5, 4496.
15 M. Choi, D. Choi, M. Jin, I. Kim, S. Kim, J. Choi, S.Y. Lee, J.M. Kim, and S. Kim, *Adv. Mater*., 2009, 21, 2185.
16 K. Takei, T. Takahashi, J. C. Ho, H. Ko, A. G. Gillies, P. W. Leu, R. S. Fearing, and A. Javey, *Nature Mater*., 2010, 9, 821.
17 H. Tian, Y. Shu, Y. Cui, W. Mi, Y. Yang, D. Xie and T. Ren, *Nanoscale*, 2014, 6, 699.
18 C. Wang, D. Hwang, Z. Yu, K. Takei, J. Park, T. Chen, B. Ma, and A. Javer, *Nat. Mater*., 2013, 12, 899.
19 J. Lee, H. Kwon, J. Seo, S. Shin, J. Koo, C. Pang, S. Son, J. Kim, Y. Jang, D. Kim, and T. Lee, *Adv. Mater*., 2015, DOI: 10.1002/adma.201500009.
20 F. Fan, L. Lin, G. Zhu, W. Wu, R. Zhang, and Z. Wang, *Nano Lett.*, 2012, 12, 3109.
21 Z. Wang, *ACS Nano*, 2013, 7, 9533.
22 Z. Wang, and J. Song, Science, 2006, 312, 242.
23 X. He, H. Guo, X. Yue, J. Gao, Y. Xia and C. Hu, *Nanoscale*, 2015, 7, 1896.
24 Y. Tai, and Z. Yang, *J. Mater. Chem*., 2011, 21, 5938.
25 Y. Li, Y. Wu, and S. Beng, *J. Am. Chem. Soc*., 2005, 127, 3266.
26 M. Li, H. X. Tang, and M. L. Roukes, *Nature nanotech*., 2007, 2, 114.
27 S. Mannsfeld, B.Tee, R.Stoltenberg, C. Chen, S. Barman, B. Muir, A. Sokolov, C. Reese, and Z. Bao. *Nature Mater*., 2010, 9, 859.
28 W. Xuan, X. He, J. Chen, W. Wang, X. Wang, Y. Xu, Z. Xu, Y.Q. Fu and J.K. Luo, *Nanoscale*, 2015, 7, 7430.
29 C. Stefan, T. Benjamin, M. Randall, V. Christopher, B. Soumendra, V. Beinn. N. Anatoliy, R. Colin, and Z. Bao, *Nat. Mater*., 2010, 9, 859.
30 Z, Keren, N. Harald, B. Yael, S. Laura, J. Paul, P. Thomas, H. Mechael, S. Robert, E. Annelise, and S. Sanjiv, *Biomaterials*, 2014, 35, 3736.
31 J. Sun, X. Zhao, W. Illeperuma, O. Chaudhuri, K. Oh, D. Mooney, J. Vlassak, and Z. Suo, *Nature*, 489, 133.
32 S. Vijoya, and G. Konstantin, *Carbon*, 2011, 49, 1859.
33 S. Yao, and Y. Zhu, *Nanoscale*, 2014, **6**, 2345
34 B. Yang, F. Guo, Y. Yuan, Z. Xiao, Y. Lu, Q. Dong, and J. Huang, Adv. Mater. 2013, 25, 572
35 M.S. Islam, M. Ashaduzzaman, A.M. Masum, and J.H. Yeum, *Dhaka Univ. J. Sci*., 2012, 60, 125.
36 P. Zhang, P.E. Lammenrt, and V.H. Crespi, *Phys. Rev. Lett*., 1998, 81, 5346.
37 B. Wei, J. Wang, Z. Chen, and G. Chen, *Chem. Eur. J*., 2008, 14, 9779.
38 H.Y. Zhao, W. Zheng. Z.X. Meng. H.M. Zhou, X.X. Xu. Z. Li, and Y.F. Zheng, *Biosens. Bioelectron.*, 2009, 24, 2352.
39 K.K. Liu, D.R. Williams, and B.J. Briscoe, *J. Phys. D: Appl. Phys*., 1998, 31, 294.
40 Y.R. Jeng, and P.Y. Wang, *J. Tribol*., 2003, 125, 232.
41 K. Kohara, Y. Tabara, A. Oshiumi, Y. Miyawaki , T. Kobayashi, and T. Miki, *Am. J. Hypertens.*, 2005, 18, 11.
42 J. Wang, J. Jiu, M. Nogi, T. Sugahara, S. Nagao, H. Koga, P. He, and K. Suganuma, *Nanoscale*, 2015, 7, 2926.
43 H. Yao, J. Ge, C. Wang, X. Wang, W. Hu , Z. Zheng, Y. Ni, and S. Yu, *Adv. Mater*., 2013, 25, 6692.

Table of content